ChemComm

COMMUNICATION

View Article Online
View Journal

Cite this: DOI: 10.1039/c4cc01962h

Received 17th March 2014,
Accepted 12th May 2014

DOI: 10.1039/c4cc01962h

www.rsc.org/chemcomm

A highly efficient mesoscopic solar cell based on $CH_3NH_3PbI_{3-x}Cl_x$ fabricated *via* sequential solution deposition†

Yingzhuang Ma,[a] Lingling Zheng,[a] Yao-Hsien Chung,[a] Saisai Chu,[a] Lixin Xiao,*[ab] Zhijian Chen,[ab] Shufeng Wang,[ab] Bo Qu,[ab] Qihuang Gong,[a] Zhaoxin Wu*[c] and Xun Hou[c]

A mixed halide perovskite of $CH_3NH_3PbI_{3-x}Cl_x$ is synthesized *via* two-step sequential solution deposition by using a mixture of $PbCl_2$ and PbI_2 as the precursor to overcome the low solubility of pure $PbCl_2$ with easy morphology control. 11.7% power conversion efficiency is achieved for the mesoscopic cell, much higher than the cell constructed *via* a spin-coating process.

Hybrid perovskite materials in the form of AMX_3 ($A = CH_3NH_3^+$; $M = Pb^{2+}$, or Sn^{2+}; and $X = Cl^-$, Br^-, or I^-) were first discovered by Weber and developed by Mitzi *et al.*, and then $CH_3NH_3PbI_3$ or $CH_3NH_3PbBr_3$ was used as the dye-absorbing layer in a liquid dye-sensitized solar cell (DSC) reported by Miyasaka *et al.*[1–3] Following the pioneering work, the perovskites were used in solid-state solar cells to avoid the dissolution of perovskite in the presence of a liquid electrolyte. As a result, much higher power conversion efficiencies (PCEs) were achieved than those of liquid cells.[4–22] Recently, Snaith *et al.* found that the electron–hole diffusion lengths exceeded 1 μm for the mixed halide perovskite of $CH_3NH_3PbI_{3-x}Cl_x$, while it was only 100 nm for the triiodide perovskite of $CH_3NH_3PbI_3$, showing the promising prospects of $CH_3NH_3PbI_{3-x}Cl_x$.[8] The mixed halide perovskite $CH_3NH_3PbI_{3-x}Cl_x$ achieved 15.4% PCE through mix-vapor vacuum deposition to give a uniform perovskite film with a planar heterojunction.[10] However, vacuum deposition will greatly increase the cost of large-scale fabrication compared to the cost-effective solution process. Up to now, spin-coating deposition has been widely used for the fabrication of solution-based $CH_3NH_3PbI_{3-x}Cl_x$ cells, but only 7.6% PCE for the $CH_3NH_3PbI_{3-x}Cl_x$ cell containing the mesoporous TiO_2 layer.[4] While $CH_3NH_3PbI_3$ devices with shorter diffusion lengths achieved the efficiencies over 15% by two-step sequential solution deposition, with easier morphology control.[7,22] The morphology of the resultant perovskite film is very sensitive to the conditions during the spin-coating procedure, *e.g.*, thickness of the compact TiO_2 layer, annealing time, annealing tempreture and the thickness of the perovskite layer.[15] The morphology of the perovskite is crucial to the device performance, because the defects in perovskite crystallites and the interfaces may be the trap of charges, preventing them reaching the electrodes. Therefore, it is necessary to improve the morphology of the $CH_3NH_3PbI_{3-x}Cl_x$ cell through the solution-based method.

To further improve the photovoltaic performance of mixed halide perovskite of $CH_3NH_3PbI_{3-x}Cl_x$ *via* the solution process, in this work, we successfully figure out the feasible compositions of the precursor for the $CH_3NH_3PbI_{3-x}Cl_x$ perovskite by two-step sequential deposition, permitting much easier morphology control. A mixture precursor of PbI_2 and $PbCl_2$ is more promising for the preparation of $CH_3NH_3PbI_{3-x}Cl_x$ than pure $PbCl_2$, due to the poor solubility of pure $PbCl_2$. The device performance reaches 11.7%, which is the highest efficiency for $CH_3NH_3PbI_{3-x}Cl_x$ *via* the solution process containing a mesoporous TiO_2 layer based on our knowledge, much higher than 4.8% for the device fabricated *via* spin-coating deposition.

The $CH_3NH_3PbI_{3-x}Cl_x$ perovskite was first reported by Snaith *et al.* by using a mixture of CH_3NH_3I and $PbCl_2$ with a molar ratio of 3 : 1 *via* spin-coating deposition (Scheme 1b).[4,5,8] Following this reaction, we first tried to use saturated (0.5 M) $PbCl_2$ as the precursor in the two-step sequential deposition, and spin-coated it on the mesoporous TiO_2 film, and then dipped into CH_3NH_3I

$$2\,CH_3NH_3I + PbCl_2 + PbI_2 \rightarrow 2\,CH_3NH_3PbI_{3-x}Cl_x \quad (a)$$

$$3\,CH_3NH_3I + PbCl_2 \rightarrow CH_3NH_3PbI_{3-x}Cl_x + CH_3NH_3I\uparrow + CH_3NH_3Cl\uparrow \quad (b)$$

Scheme 1 The reactions for $CH_3NH_3PbI_{3-x}Cl_x$.

[a] State Key Laboratory for Mesoscopic Physics and Department of Physics, Peking University, Beijing 100871, PR China. E-mail: xiao66@pku.edu.cn
[b] New Display Device and System Integration Collaborative Innovation Center of the West Coast of the Taiwan Strait, Fuzhou 350002, China
[c] Key Laboratory of Photonics Technology for Information, Key Laboratory for Physical Electronics and Devices of the Ministry of Education, Department of Electronic Science and technology, School of Electronic and Information Engineering, Xi'an Jiaotong University, Xi'an, 710049, PR China. E-mail: zhaoxinwu@mail.xjtu.edu.cn

† Electronic supplementary information (ESI) available: Material synthesis, EDX results, device preparation procedures, and device characterization. See DOI: 10.1039/c4cc01962h

solution to form perovskite on site. Unfortunately, the absorption of the resultant film was very weak. It might be due to the poorer solubility of $PbCl_2$ than that of PbI_2 in dimethylformamide (DMF), because high concentration (at least 1 M) of the precursor is very important to obtain high loading in the mesoporous TiO_2 film for high device performance.[7] However, in the presence of additives, *e.g.*, PbI_2 or CH_3NH_3I, the solubility of $PbCl_2$ can be significantly increased due to the common ion effect.[15,31] In addition, the higher formation energy of chlorine incorporation into the perovskite matrix than that of iodine might also be the reason.[26] Therefore, we changed the precursor to a mixture of 0.5 M $PbCl_2$ and 0.5 M PbI_2 (molar ratio 1 : 1) according to the reaction of Scheme 1a, and followed the two-step sequential deposition to give Film a with the color changing from chartreuse to dark brown, indicating the formation of the perovskite. From the reaction formula given below, it could also be inferred that Scheme 1a tends to give less byproducts compared to Scheme 1b. The excess methylammonium iodide and chloride are assumed to be lost *via* evaporation during the annealing process.[4] Less byproducts may leave fewer pin-holes in the perovskite layer during the annealing process.[15] As comparison, the resultant film formed by using $PbCl_2$ as the precursor (Scheme 1b) is referred to as Film b. The illustrations of different fabrication procedures for $CH_3NH_3PbI_{3-x}Cl_x$ layers are shown in Fig. 1.

The structures of the resultant perovskite films were investigated *via* X-ray diffraction (XRD) as shown in Fig. 2a. The structure of the synthesized perovskite is consistent with tetragonal phase structures reported in the previous reports.[23–25] Strong peaks at 14.03° and 27.52°, corresponding to the (110) and (220) planes, confirm the formation of a tetragonal perovskite structure with lattice parameters $a = b = 8.84$ Å and $c = 12.57$ Å. The signals of Film b are much weaker than those of Film a, indicating that more perovskite crystallites formed in mesoporous TiO_2 by the mixture of PbI_2 and $PbCl_2$ than pure $PbCl_2$ as the precursor. The composition of Film a was confirmed by the energy-dispersive X-ray (EDX) spectrum as shown in Fig. S1 (ESI†). The elemental mapping analysis of the surface confirms that the resultant perovskite of Film a is a mixed halide $CH_3NH_3PbI_{3-x}Cl_x$ with approximately $x \approx 0.26$. The images of Pb, I and Cl also show that the perovskites are well distributed. The absorption spectra of the two perovskite films are shown in Fig. 2b. Film a has strong broadband absorption in the visible region from 400 nm to 800 nm, on the contrary, Film b has rather poor absorption, indicating insufficient perovskite filling in the porous TiO_2 layer. These results indicate that using the mixture of PbI_2 and $PbCl_2$ as the precursor is an effective way to form the mixed halide perovskite of $CH_3NH_3PbI_{3-x}Cl_x$, following Scheme 1a.

To further evaluate the differences in the resultant $CH_3NH_3PbI_{3-x}Cl_x$ perovskite layers between two-step sequential deposition and spin-coating deposition, we also fabricated another perovskite layer *via* spin-coating the mixture of CH_3NH_3I, $PbCl_2$ and PbI_2 (molar ratio 2 : 1 : 1) also following Scheme 1a for comparison (hereafter referred to as Film c). The morphology of Film a, Film b and Film c was measured by both scanning electron microscopy (SEM) and atomic force microscopy (AFM) as shown in Fig. 3.

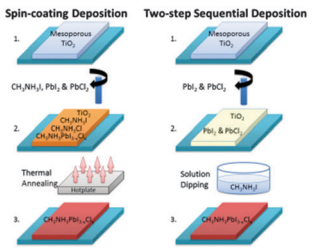

Fig. 1 The illustrations of fabrication procedures of the provskite layer fabricated *via* spin-coating deposition and two-step sequential deposition.

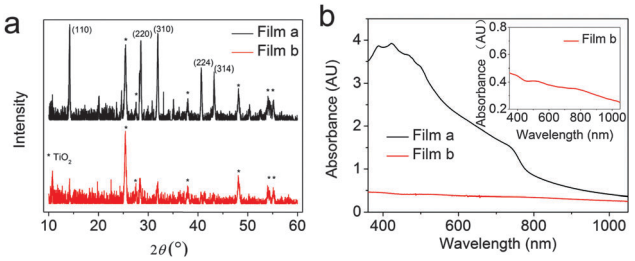

Fig. 2 (a) XRD spectra of Film a and b. (b) Absorbance of Film a and b.

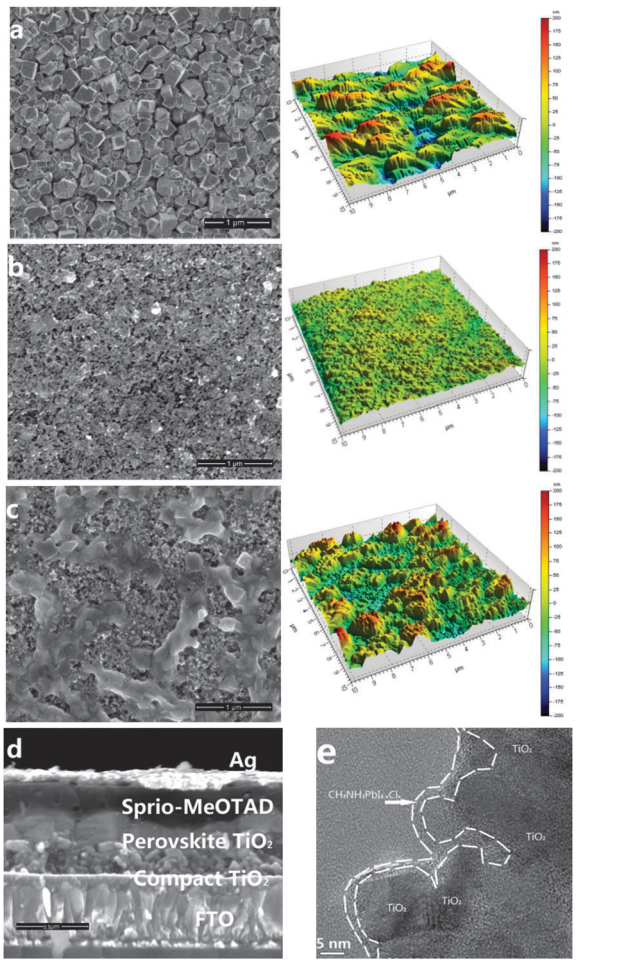

Fig. 3 The SEM and AFM images of (a) Film a, (b) Film b and (c) Film c. (d) The cross-sectional SEM view of Device A. (e) TEM images of $CH_3NH_3PbI_{3-x}Cl_x$ deposited in the mesoporous TiO_2 film.

By using the mixture of PbI_2 and $PbCl_2$ as the precursor (Film a), the perovskite *via* two-step sequential deposition did not only penetrate deeply into the mesoporous TiO_2, but also grew into crystallites to cover the TiO_2 layer with an in-plain grain size of 300–350 nm as shown in Fig. 3a, and the grain size has been proved to be suitable with a strong light scattering effect to further enhance the light absorption.[30] On the contrary, there were almost no more perovskite crystallites on top of the mesoporous TiO_2 for Film b fabricated *via* two-step sequential deposition by using $PbCl_2$ as the precursor as shown in Fig. 3b, indicating insufficient pore filling in the mesoporous TiO_2 layer. This might be one of the possible reasons for the absorption difference by using different precursors. For Film c, the SEM images (Fig. 3c) showed that no continuous perovskite capping layer was formed on top of the mesoporous TiO_2, although there was penetration into the mesoporous TiO_2 layer. The above results indicate that the morphology of the perovskite layer fabricated *via* two-step sequential deposition is easier to control compared with *via* spin-coating deposition. The surface morphology of the three films was also investigated *via* AFM images. As a result, the crystalline arrangement in Film a formed a continuous microstructure consistent with the SEM image, the absorption of incident light was enhanced due to the presence of the crystalline perovskite capping layer and the light scattering effect, which have also been proved to be an effective way in DSCs.[22,27] These results could be proved by the cross-section image (Fig. 3d) with elemental mapping (Fig. S2, ESI†) of Film a. It could be clearly identified that the perovskite not only formed a continuous capping layer, but also penetrated well into the mesoporous TiO_2 film. The perovskite pore-filling should improve the device performance because higher electron densities can be sustained in the TiO_2 layer, increasing electron transporting rates as previously reported.[28] To further evaluate the interfacial properties of TiO_2/perovskite, the transmission electron microscopy (TEM) image (Fig. 3e) was obtained from the scratch from Film a. The image reveals the formation of the $CH_3NH_3PbI_{3-x}Cl_x$ perovskite thin film on the TiO_2 surface, which prohibits the direct contact between TiO_2 and hole transporting material (HTM).

The experimental details of device fabrication are given in the ESI.† Devices A and B correspond to Film a and Film c, respectively. Devices were measured under a standard AM 1.5 illumination of 100 mW cm^{-2}. The *J–V* curves are shown in Fig. 4a. The incident photon to current conversion efficiency (IPCE) was measured as shown in Fig. 4b.

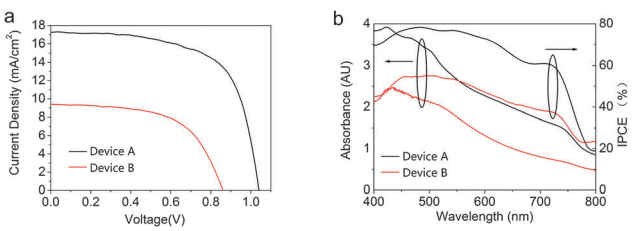

Fig. 4 (a) The photovoltaic performances of Devices A and B. (b) Absorbance and IPCE of the perovskite films in Devices A and B.

Table 1 Photovoltaic performances of the hybrid perovskite solar cells

Device	Process	V_{oc} [V]	J_{sc} [mA cm^{-2}]	FF	PCE [%]
A	Sequential	1.04	17.2	0.65	11.7
B	Spin-coating	0.86	9.4	0.59	4.8
Ref. 10	Vacuum	1.07	21.5	0.67	15.4
Ref. 4	Spin-coating	0.80	17.8	0.53	7.6

Compared with Device B, the IPCE of Device A is over 60% between 400 to 700 nm, and the highest value is nearly 80% at around 500 nm, matching the stronger absorption region of the perovskite layer. The PCE of Device A is up to 11.7%, with a J_{sc} of 17.2 mA cm^{-2}, a V_{oc} of 1.04 V, and a FF of 0.65, which is the highest efficiency for $CH_3NH_3PbI_{3-x}Cl_x$ *via* the solution process containing a mesoporous TiO_2 layer based on our knowledge, much higher than that of 7.6% obtained *via* the spin-coating process with the mesoporous TiO_2 layer as reported listed in Table 1.[4] The corresponding Device B showed a J_{sc} of 9.4 mA cm^{-2}, a V_{oc} of 0.86 V, a FF of 0.59 and 4.8% PCE (Fig. 4a), a much lower PCE than that of the Device A fabricated *via* two-step sequential deposition. The improvement of photovoltaic performances may be mainly ascribed to the different perovskite morphology of the two devices. Compared with Device A, there is 0.18 V decrease in the V_{oc} of Device B because of the direct contact between the uncovered TiO_2 and the p-type HTM due to the absence of the perovskite capping layer, resulting in the charge recombination between the TiO_2 and HTM.[15,28,29] Besides, the absence of the perovskite capping layer might lead to lower absorption, resulting in lower J_{sc}. It should be noted here that the lower PCE than 15% for $CH_3NH_3PbI_3$ *via* two-step sequential deposition might be due to the lower solubility of $PbCl_2$ than that of PbI_2 in the solvent of DMF. High concentration should be crucial to the growth of perovskite crystallites as reported in the case of $CH_3NH_3PbI_3$ *via* two-step sequential deposition.[7] This could be also supported by the lower PCEs for $CH_3NH_3PbI_{3-x}Cl_x$ *via* the solution process than that *via* vacuum deposition (sufficient chlorine source). Compared to the $CH_3NH_3PbI_{3-x}Cl_x$ cell with 15.4% PCE fabricated *via* vacuum deposition, the V_{oc} and the FF of the spin-coated $CH_3NH_3PbI_{3-x}Cl_x$ cells are significantly lower, due to the difficulty in controlling the morphology of the perovskite crystallites formed *via* a spin-coating process, leading to the lower PCE of 7.6%. While Device A fabricated *via* two-step sequential deposition is an effective method to reduce the V_{oc} and FF losses caused by the morphology defects of $CH_3NH_3PbI_{3-x}Cl_x$ perovskite. Further work should be focused on optimizing the conditions to control the morphology of the perovskite capping layer to further increase the lower J_{sc} caused by the low solubility of $PbCl_2$ as mentioned above.

In conclusion, we introduce two-step sequential solution deposition for the fabrication of the $CH_3NH_3PbI_{3-x}Cl_x$ mesoscopic solar cell. The mixture of PbI_2 and $PbCl_2$ is used rather than pure $PbCl_2$ as the precursor to ensure high loading in the mesoporous TiO_2 film, with easy morphology control, which results in a great enhancement of the light absorbance for the device and suppressing the electron hole recombination by separating the bare TiO_2 and the HTM layer. As a result, 11.7% PCE for the device has been achieved with a J_{sc} of 17.2 mA cm^{-2},

a V_{oc} of 1.04 V of, and a FF of 0.6, which is the highest efficiency of $CH_3NH_3PbI_{3-x}Cl_x$ fabricated *via* a solution process containing a mesoporous TiO_2 layer based on our knowledge. This is much higher than 4.8% for the device fabricated *via* a spin-coating process. This work suggests a promising way for the solution-based preparation of the mixed halide perovskite of $CH_3NH_3PbI_{3-x}Cl_x$ for highly efficient solar cells.

This study was partly financially supported by the National Natural Science Foundation of China (10934001, 61177020, 11074016, 11121091, 61275034 and 61106123) and the National Basic Research Program of China (2013CB328700). The authors are thankful to Mr Xiao Yu and Prof. Dechun Zou in the College of Chemistry and Molecular Engineering of Peking University for their kind help with the measurements of SEM images.

Notes and references

1 D. Weber, *Z. Naturforsch., B: Anorg. Chem. Org. Chem.*, 1978, **33**, 1443.
2 D. B. Mitzi, C. A. Field, W. T. A. Harrison and A. M. Guloy, *Nature*, 1994, **369**, 467.
3 A. Kojima, K. Teshima, Y. Shirai and T. Miyasaka, *J. Am. Chem. Soc.*, 2009, **131**, 6050.
4 M. M. Lee, J. Teuscher, T. Miyasak, T. N. Murakami and H. J. Snaith, *Science*, 2012, **338**, 643.
5 J. M. Ball, M. M. Lee, A. Hey and H. J. Snaith, *Energy Environ. Sci.*, 2013, **6**, 1739.
6 H. S. Kim, C. R. Lee, J. H. Im, K. B. Lee, T. Moehl, A. Marchioro, S. J. Moon, R. H. Baker, J. H. Yum, J. E. Moser, M. Grätzel and N. G. Park, *Sci. Rep.*, 2012, **2**, 591.
7 J. Burschka, N. Pellet, S. J. Moon, R. Humphry-Baker, P. Gao, M. K. Nazeeruddin and M. Grätzel, *Nature*, 2013, **499**, 316.
8 S. D. Stranks, G. E. Eperon, G. Grancini, C. Menelaou, M. J. Alcocer, T. Leijtens and H. J. Snaith, *Science*, 2013, **342**, 341.
9 G. Xing, N. Mathews, S. Sun, S. S. Lim, Y. M. Lam, M. Grätzel and T. C. Sum, *Science*, 2013, **342**, 344.
10 M. Liu, M. B. Johnston and H. J. Snaith, *Nature*, 2013, **501**, 395.
11 L. Etgar, P. Gao, Z. Xue, Q. Peng, A. K. Chandiran, B. Liu and M. Grätzel, *J. Am. Chem. Soc.*, 2012, **134**, 17396.
12 D. Bi, L. Yang, G. Boschloo, A. Hagfeldt and E. M. Johansson, *J. Phys. Chem. Lett.*, 2013, **4**, 1532.
13 D. Sabba, H. M. Kumar, N. Yantara, T. T. T. Pham, N. G. Park, M. Grätzel and P. P. Boix, *Nanoscale*, 2014, **6**, 1675.
14 M. H. Kumar, N. Yantara, S. Dharani, M. Grätzel, S. Mhaisalkar, P. P. Boix and N. Mathews, *Chem. Commun.*, 2013, **49**, 11089.
15 G. E. Eperon, V. M. Burlakov, P. Docampo, A. Goriely and H. J. Snaith, *Adv. Funct. Mater.*, 2014, **24**, 151.
16 J. Y. Jeng, Y. F. Chiang, M. H. Lee, S. R. Peng, T. F. Guo, P. Chen and T. C. Wen, *Adv. Mater.*, 2013, **25**, 3727.
17 J. H. Heo, S. H. Im, J. H. Noh, T. N. Mandal, C. S. Lim, J. A. Chang and S. I. Seok, *Nat. Photonics*, 2013, **7**, 486.
18 H. S. Kim, J. W. Lee, N. Yantara, P. P. Boix, S. A. Kulkarni, S. G. Mhaisalkar and N. G. Park, *Nano Lett.*, 2013, **13**, 2412.
19 A. Abrusci, S. D. Stranks, P. Docampo, H. L. Yip, A. K. Y. Jen and H. J. Snaith, *Nano Lett.*, 2013, **13**, 3124.
20 N. G. Park, *J. Phys. Chem. Lett.*, 2013, **4**, 2423.
21 J. Burschka, A. Dualeh, F. Kessler, E. Baranoff, N. L. Cevey-Ha, C. Yi and M. Grätzel, *J. Am. Chem. Soc.*, 2011, **133**, 18042.
22 D. Liu and T. L. Kelly, *Nat. Photonics*, 2014, **8**, 133.
23 T. Baikie, Y. Fang, J. M. Kadro, M. Schreyer, F. Wei, S. G. Mhaisalkar and T. J. White, *J. Mater. Chem. A*, 2013, **1**, 5628.
24 C. C. Stoumpos, C. D. Malliakas and M. G. Kanatzidis, *Inorg. Chem.*, 2013, **52**, 9019.
25 S. Colella, E. Mosconi, P. Fedeli, A. Listorti, F. Gazza, F. Orlandi, P. Ferro, T. Besagni, A. Rizzo, G. Calestani, G. Gigli, F. D. Angelis and R. Mosca, *Chem. Mater.*, 2013, **25**, 4613.
26 E. Mosconi, A. Amat, M. K. Nazeeruddin, M. Grätzel and F. D. Angelis, *J. Phys. Chem. C*, 2013, **117**, 13902.
27 S. Hore, P. Nitz, C. Vetter, C. Prahl, M. Niggemann and R. Kern, *Chem. Commun.*, 2005, 2011.
28 T. Leijtens, B. Lauber, G. E. Eperon, S. D. Stranks and H. J. Snaith, *J. Phys. Chem. Lett.*, 2014, **5**, 1096.
29 H. J. Snaith, N. C. Greenham and R. H. Friend, *Adv. Mater.*, 2004, **16**, 1641.
30 Q. Chen, H. Zhou, Z. Hong, S. Luo, H.-S. Duan, H.-H. Wang, Y. Liu, G. Li and Y. Yang, *J. Am. Chem. Soc.*, 2013, **136**, 622.
31 J. Mendham, R. C. Denney, J. D. Barnes and M. J. K. Thomas, *Vogel's Quantitative Chemical Analysis*, Prentice Hall, New York, 6th edn, 2000, ISBN 0-582-22628-7.

